

# Understanding Droplet Collisions through a Model Flow: Insights from a Burgers Vortex

Lokahith Agasthya,<sup>1,2,3,\*</sup> Jason R. Picardo,<sup>2,†</sup> S. Ravichandran,<sup>4,‡</sup> Rama Govindarajan,<sup>2,§</sup> and Samridhhi Sankar Ray<sup>2,¶</sup>

<sup>1</sup>Indian Institute for Science Education and Research, Pune, 411008, India

<sup>2</sup>International Centre for Theoretical Sciences, Tata Institute of Fundamental Research, Bangalore 560089, India

<sup>3</sup>Department of Physics and INFN, University of Rome Tor Vergata, Via della Ricerca Scientifica 1, 00133 Rome, Italy

<sup>4</sup>Nordita, KTH Royal Institute of Technology and Stockholm University, 10691 Stockholm, Sweden

We investigate the role of intense vortical structures, similar to those in a turbulent flow, in enhancing collisions (and coalescences) which lead to the formation of large aggregates in particle-laden flows. By using a Burgers vortex model, we show, in particular, that vortex stretching significantly enhances sharp inhomogeneities in spatial particle densities, related to the rapid ejection of particles from intense vortices. Furthermore our work shows how such spatial clustering leads to an enhancement of collision rates and extreme statistics of collisional velocities. We also study the role of poly-disperse suspensions in this enhancement. Our work uncovers an important principle which, if valid for realistic turbulent flows, may be a factor in how small nuclei water droplets in warm clouds can aggregate to sizes large enough to trigger rain.

## I. INTRODUCTION

The transport of small, often spherical, particles in turbulent flows are central to several processes in nature and industry. These phenomena span across several orders of length and time scales and are of importance for problems in statistical physics, fluid dynamics, geophysics as well as astrophysics. More often than not, such particles are neither massless nor point-like (tracers): Hence our understanding of the anomalous nature of Lagrangian turbulence is often inadequate when dealing with small, but finite-sized, heavy particles [1]. This is because such *inertial* particles—embryonic rain drops in a warm cloud [2–4], pollen grains and pollutants [5, 6], or even planetesimals in a dusty circumstellar disk of gas [7]—behave very differently from tracers in a flow. A key *difference* between the dynamics of tracers and inertial particles is *dissipation*: The phase space for tracers is conserved whereas that associated with inertial particles shrinks [1]. A dramatic visual manifestation of this is seen, e.g., in a snapshot of an ensemble of inertial particles in a flow. Such configurations show an inhomogeneous, preferential concentration of the particles in certain regions of the flow unlike the case of tracers which distribute homogeneously [8–11].

Amongst the several problems of interest in this field, a recent focus has been on the issues of collisions [12–19], coalescences [2, 4, 12, 20] and settling [3, 21] of such particles in a turbulent flow. Although such questions are important for fluid dynamics and the statistical physics of non-equilibrium transport and aggregation problems, there has also been a greater appreciation for its implication in understanding, e.g., the microphysics of droplet growth leading to precipitation in warm clouds. This is because the growth of water droplets from small aerosols is, beyond a certain size, dominated by coalescence. Hence the role of turbulent fluctuations in broad-

ening the size distribution of droplets, beginning with, e.g., a mono-disperse suspension of particles, deserves attention.

How effective is turbulence-driven coalescence in triggering the growth of large objects? The answer to this question must depend on the way particles approach each other. This rate of approach has its origins in two distinct features of particle dynamics, namely, preferential concentration leading to an inhomogeneous distribution of particles, and sling or caustic effects [22–24] which cause heavy particles, of suitable sizes, to collide with unusually large velocity differences. A mechanical interpretation of both these effects can be traced back to the proliferation of vortices in a three-dimensional flow: Vortices in a flow act like centrifuges, expelling heavy particles from their core. Hence particles are seen to cluster in regions of low rotation and high strain. Furthermore, expelled particles which are sufficiently large (yet smaller than the Kolmogorov scale of the flow) can meet other particles with arbitrary (and hence often large) velocity differences, and thereby collide rapidly. However, the precise role of the curious inter-twined geometry of straining and vortical regions in particle-collisions has been examined in fully developed three-dimensional turbulent flows, via direct numerical simulations, only recently [19]. The probability of coalescence upon collision of two droplets is a complex issue, beyond the scope of this paper.

The question remains, however, of the precise importance of vortical structures in facilitating droplet growth, especially when the carrier flows are strongly turbulent. A clear, definitive answer is difficult for two principal reasons. Firstly, full-resolved numerical simulations can rarely reach Reynolds numbers which are large enough for us to isolate the role of vortices with a high degree of satisfaction. Secondly, inertial particles have non-trivial correlations with the advecting flow: This makes it hard to isolate the effect of vortical ejections of particles on collisions and coalescence.

Nevertheless, this question is an important one, especially if we want to understand natural phenomena, such as droplet growth in warm clouds. Such clouds are highly turbulent, and the role of vortices needs to be examined with care. However, such Reynolds numbers are beyond the reach of fully-resolved simulations, based on the Navier-Stokes equations. Hence the need to examine reduced models to shed light on this phe-

\* lnagasthya@gmail.com

† jrpicardo@icts.res.in

‡ ravichandran@su.se

§ rama@icts.res.in.com

¶ samridhhisankarray@gmail.com

nomenon.

A first step in this direction, by Ravichandran and Govindarajan [25] (and later developed in Ref. [20]), was the use of particles interacting *only* with a two-dimensional stationary point or Gaussian vortices. Their work uncovered two important aspects of vortex-particle interactions. Firstly, it was shown that caustics, defined as the co-existence at some physical location of two particles with different velocities, occur only if (a) at least one of the particles started within a critical radius  $r_{cr}$  of the centre of the vortex and (b) the particle Stokes number, to be defined precisely later, is greater than a critical value  $St_{cr}$ . Secondly, as a consequence of this, particles starting near a vortex undergo significantly more collisions as they are expelled out, than particles starting far from the vortex.

In this paper, we extend these ideas concretely in a three-dimensional set-up with stretched Burgers vortices. In particular, we elucidate the complementary roles of axial straining and intense vorticity in enhancing collision rates, primarily through the mechanism of *slings* [14].

Before we get into a detailed description of the model and our results, it would be useful at this stage to stress that the Burgers vortex, despite its simplicity and limited connection with the phenomenology of three-dimensional turbulence, has been an important testing ground for several ideas for the mathematical and fluid dynamical aspects of the Navier-Stokes equation. The Burgers vortex [26], being an exact solution of the Navier-Stokes equation, is an important model for self-similar flows which are stationary, where the intensification of vorticity due to the axial straining flow—leading to sharp columnar structures—is balanced by viscous diffusion. This is indeed reminiscent of extended vorticity filaments seen in turbulent flows, both numerically [27–29] and in experiments [30]. Consequently, it serves as an important model for vortex stretching—a uniquely three-dimensional phenomena—and hence for fundamental mathematical studies of (dissipative) Euler and Navier-Stokes solutions [31–34]. Moreover, ensembles of such model vortices have been shown to provide a reasonable approximation, and hence a testing ground, for realistic turbulent flows [35]. This has motivated earlier authors to use such models for understanding problems of Lagrangian turbulence [36] as well as turbulent transport of heavy inertial particles [37, 38]. In a similar spirit, we analyze the relative motion of droplets suspended in and around a Burgers vortex, in order to gain insight into the enhancement of droplet collisions by intense vortical structures in turbulent flows.

The rest of the paper is organised as follows. In Sec. II, we describe our model of the Burgers vortex interacting with inertial particles, as well as the parameters that we use. We then describe the results we obtain from our detailed numerical simulations in Sec. III and conclude with discussions—especially the relevance of these results to the problem of droplet growth in warm clouds—in Sec. IV.

## II. THE BURGERS VORTEX MODEL

We consider a single, cylindrically symmetric, three-dimensional, *stationary*, model vortex such that the vorticity is maximum at its centre and falls off as we move away from the core. Such a Burgers vortex [26], centered at the origin and aligned along the  $\hat{z}$ -axis (without any loss of generality), and characterised by its circulation  $\Gamma$  and radius  $r_{core}$ , is best described through the velocity field written in cylindrical coordinates (and in component form):

$$u_\theta = \frac{\Gamma}{2\pi r} \left( 1 - \exp\left(-\frac{r^2}{r_{core}^2}\right) \right); \quad (1a)$$

$$u_r = -\sigma r; \quad (1b)$$

$$u_z = 2\sigma z. \quad (1c)$$

This structure of the velocity field, along with the stretching coefficient  $\sigma$ , ensures outward stretching along the  $\hat{z}$ -axis, accompanied by a radially inward component as demanded by incompressibility. Therefore, for small values of  $r$ , i.e., close to the vortex core, the tangential velocity  $u_\theta$  dominates and the flow is mostly rotational; at large distances  $r$ , however, the radially-inward, axially-outward straining flow dominates. Such a flow (1) leads to a vorticity field, which has a single non-trivial (Gaussian)  $z$ -component, given by [39]

$$\omega_z = \frac{\Gamma}{\pi r_{core}^2} \exp\left(-\frac{r^2}{r_{core}^2}\right). \quad (2)$$

We now seed heavy inertial particles near the origin, with an initial velocity that matches the velocity of the fluid at that position. The dynamics of such small, dense, spherical particles is defined by the linear Stokes drag model:

$$\begin{aligned} \frac{d\mathbf{x}}{dt} &= \mathbf{v}; \\ \frac{d\mathbf{v}}{dt} &= -\frac{\mathbf{v} - \mathbf{u}}{\tau_p}. \end{aligned} \quad (3)$$

This set of equations, derived from the so-called Maxey-Riley equation [40] (see also Ref. [6]), allows us to obtain the position  $\mathbf{x}$  and velocity  $\mathbf{v}$  of a given particle at any instant of time. The Stokes time  $\tau_p$ —a measure of the inertia of the particle—sets the time-scale needed by the particle to relax to the velocity of the carrier fluid. In most studies of turbulent transport, this measure of inertia is best expressed through the non-dimensional Stokes number  $St = \tau_p/\tau_\eta$ , where  $\tau_\eta$  is the so-called Kolmogorov (small-scale) time-scale of an advecting *turbulent* flow. Although we examine a model flow, it is useful to adapt this definition to make meaningful comparisons to warm clouds, where such a vortex-particle system mimics their dominant vortical structures—because of extreme Reynolds numbers—interacting with nuclei droplets. In our numerical simulations, we use a second-order Runge-Kutta scheme, with a time step  $\delta t = 10^{-3}$ , and a few values of  $\tau_p$  (see Table I), to solve the equations of motion for the particles. For well-converged statistics, we use  $N_p = 200,000$  particles for each of our simulations. It is important to point out that we report results for a rather narrow range of Stokes

Fluid (Burgers Vortex)		Particles	
Type	$r_{\text{core}}$	$\sigma$	$St$
$V_1$	0.2	0	0.03
	0.2	0.08	0.03
	0.2	0.08	0.06
	0.2	0.08	0.1
	0.2	0.25	0.03
	0.2	0.3	0.03
$V_2$	0.4	0	0.03
	0.4	0.02	0.03
	0.4	0.08	0.03
	0.4	0.25	0.03
	0.4	1.0	0.03

TABLE I. Representative list of parameters that have been used in our numerical simulations and reported in this paper.

numbers (0.03 to 0.1). This is because of two reasons. Firstly, the rather subtle effect that we are interested in is really dominant for this range of  $St$ ; the effect is inconsequential for tracers, while for finitely large values of  $St$  the ballistic motion of particles overwhelms the role played by the geometry of our model flow. Secondly, these Stokes numbers are realistic for droplet-nuclei in settings such as warm clouds, whose physics is part of the motivation for this study.

Measurements suggest a spread of the mean-energy-dissipation rates as well as the Reynolds numbers in a turbulent warm cloud. We choose a typical set of values for the mean-energy-dissipation rate  $\epsilon = 0.01\text{m}^2\text{s}^{-3}$ , and Taylor Reynolds number  $Re_\lambda = 5000$ , as well as the kinematic viscosity  $\nu = 1.48 \times 10^{-5}\text{m}^2\text{s}^{-1}$  for air. It is important to keep in mind that, given the nature of our work, the precise combination of these numbers does not fundamentally alter our results and the conclusions that we draw from them. Having measurements of  $\nu$  and  $\epsilon$ , it is trivial now to obtain the Kolmogorov length-scale  $\eta$  and time-scale  $\tau_\eta$ , as well as the spatially-averaged *enstrophy*  $\langle\omega^2\rangle = \frac{\epsilon}{\nu}$ , associated with the turbulent flow in such clouds.

These are, of course, intensely turbulent flows and our understanding of such systems suggests proliferation of intense, sharp columnar vortical structures [28], which empirically are regions of vorticity greater than  $\sqrt{\langle\omega^2\rangle Re_\lambda}$ . In this paper, it is this peculiar aspect of highly turbulent regimes that we replicate through the Burgers vortex defined earlier. We choose 2 different sets of Burgers vortices—namely a *small core* and *large core* vortex, corresponding to two different values of  $r_{\text{core}}$  (and the associated circulation  $\Gamma$  and stretching coefficient  $\sigma$ ). Our choice of parameters for our simulations is listed in Table 1, and how these dimensionless parameters are obtained from the various dimensional measurements in. e.g., a turbulent cloud, is described in Appendix A.

Finally, we seed particles with several different Stokes numbers, including the typical value of  $St = 0.03$  as commonly seen in nuclei aerosols.

### III. RESULTS

To understand the dynamics of inertial particles near a strong vortex, it is best to begin by examining single particle trajectories, starting out at an initial radial distance  $r_0$  (measured from the axis of the vortex). The time evolution of such a particle, in particular its radial distance  $r(t)$ , ought to depend on both  $r_0$  and the stretching coefficient  $\sigma$ , which counters the centrifugal effect of the vortex on the particles. In Fig. 1, we show representative plots of the radial distance  $r$  for a particle with  $St = 0.03$  at time  $t = 0.6\tau_\eta$ , for both the small ( $r_{\text{core}} = 0.2$ ) and large ( $r_{\text{core}} = 0.4$ ) core vortices (panels (a) and (b), respectively). Our results clearly show that although we expect the particles to be centrifuged out of the vortex, for sufficiently large  $\sigma$ , and  $r_0$ , the particles actually come closer to the vortex axis. To make this clear, we show, in Fig. 1, a diagonal line which serves as a guide to the eye: Portions of the curves lying above this diagonal represent particles which, for a given  $r_0$  and  $\sigma$ , centrifuge out and move away from the vortex-axis; the part of the curve lying below this diagonal correspond to the cases where  $r_0$  and  $\sigma$  conspire to pull the particles into the vortex. Particles with a sufficiently small  $r_0$  always end up moving away from the vortex and their radial distance at short times seem to be independent of  $\sigma$ , but influenced by the strength of the vortex: a smaller  $r_{\text{core}}$  (or a more *intense* vortex) leads to a more violent ejection. Interestingly, though, for a sufficiently large value of  $r_0$ , the role of  $\sigma$  becomes non-trivial. Hence, for any given initial separation  $r_0$ , particles may well be brought *inwards* if the stretching of the flow  $\sigma$  is strong enough. Of course, at very long times all particles, regardless of  $r_0$ , will asymptote to a distance  $r_\star$  determined by  $\Gamma$  and  $\sigma$ , where outward centrifugal forces are balanced by inward drag from the stretching flow [37]. We have checked that this effect is indeed independent of the Stokes numbers that we consider in this paper.

It is worth making a final comment on Fig. 1. For strong vortices (panel (a)), particles which start at different, but reasonably short distances  $r_0 \lesssim r_{\text{core}}$  end up roughly at the same  $r = r_\star \gtrsim r_{\text{core}}$ , as seen by the curves plateauing out. This in turn implies that particles which start closer to the center of the vortex have a higher speed of ejection than those that start further away. This effect naturally weakens when the strength of the vortex diminishes, as is evidenced by the absence of a similar plateau in Fig. 1(b). The differential ejection of particles, in case of a strong vortex, enables particles which begin near the vortex to overtake, in finite time, those that begin further away, resulting in the formation of caustics [25].

To understand how vortex stretching impacts the formation of caustics, we calculate the critical Stokes number,  $St_{cr} = \tau_{p,cr}/\tau_\eta$  (for the mono-disperse case). Given the vortex strength and the stretching rate, particles with  $St < St_{cr}$  will not undergo caustics. The variation of  $St_{cr}$  with the stretching rate thus quantifies the effect of stretching on caustic-formation, and is shown for the present value of  $Re_\lambda$  in Fig. 2. A scale-free version (again following the scaling used in Ref. [25]) where the dependence on the Taylor Reynolds number is apparent is shown in the Appendix. The decrease in the critical Stokes number with increasing stretch-

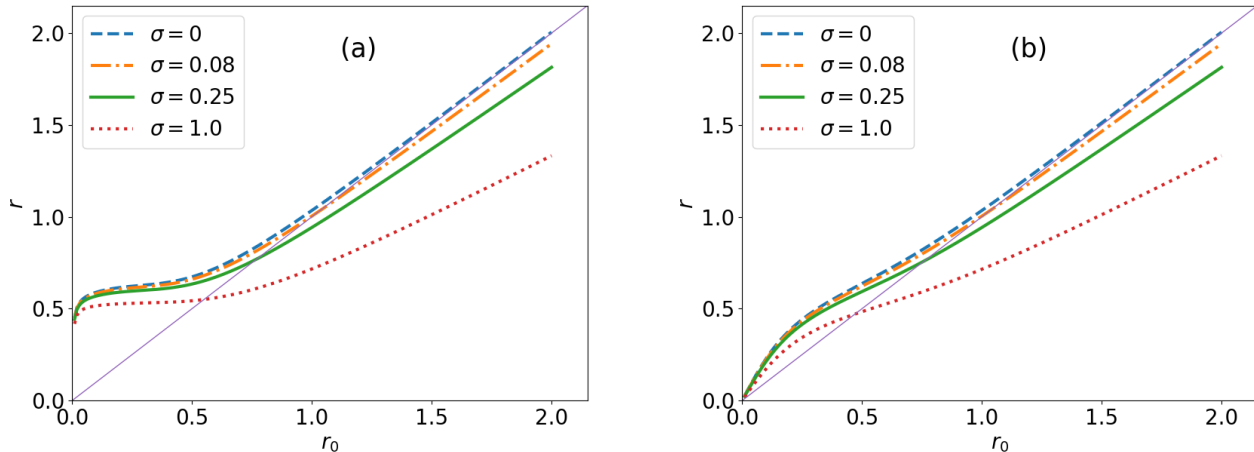


FIG. 1. (color online) Representative plots of the final radial distance  $r$  as a function of the initial radial distance  $r_0$  for particles with  $St = 0.03$  at a short time  $t = 0.6\tau_\eta$  for a (a) strong ( $r_{\text{core}} = 0.2$ ) and (b) weak ( $r_{\text{core}} = 0.4$ ) vortex. We show data for different flow geometries characterised by  $\sigma$ , and the unbroken (purple) diagonal line is a guide to the eye to differentiate particles which are centrifuged out ( $r > r_0$ ) from those which are drawn in ( $r < r_0$ ).

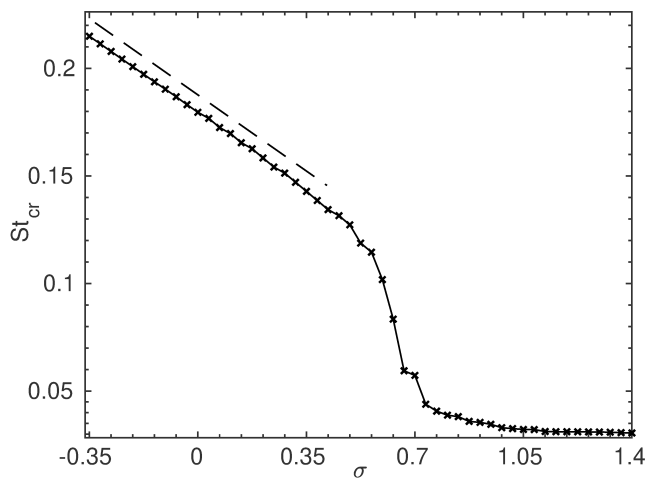


FIG. 2. The critical Stokes (see text for definition) as a function of the nondimensional stretching rate. For small stretching rates, the critical Stokes falls linearly with increasing rate (the slope of the dashed line is  $-1/10$ ). There also seems to be an asymptotic value at high stretching rates.

ing rate suggests that, for a given particle size, a vortex that is stretched will produce more caustics than a vortex that is not. We shall see below that, apart from this, the collisions at a given Stokes number are enhanced by stretching as well.

All of this suggests that the number density of particles  $\Phi$ , at some time  $t$ , should depend sensitively on  $r$ . We define this density as the ratio of the number of particles  $N(r)$  at a given  $r$  (suitably normalised and binned) to the total number

of particles  $N_p$ , *i.e.*,

$$\Phi = \frac{1}{2\pi r h} \frac{N(r)}{N_p}$$

where  $h$  is the height of the cylinder in which the particles are uniformly distributed initially.

The number density of particles  $\Phi$  is a non-stationary measure; however since we want to capture the collision statistics dominated by vortical expulsion, it is enough to measure this quantity at times that are just long enough for most of the particles to have left the vortical core and accumulate near  $r_*$ . This is because it is in this setting that collisions will be dominated by the vortical expulsion of particles. Hence, in Fig. 3, we show  $\Phi$  (for  $St = 0.03$  and averaged over 100 different initial realisations of the particles) as a function of  $r$ , at  $t = 0.6\tau_\eta$ , for different vortices and stretching rates. The time chosen here satisfies the constraint discussed earlier, without being so large as to allow particles that were initially far from the vortex to become concentrated at  $r_*$ , because of the inward flow due to straining. (We have checked that our conclusions and results (qualitatively) are unchanged for slight variations to the waiting time.)

We see clearly that starting from an initial profile in which particles are uniformly distributed in space, the particles evacuate rapidly from regions close to the core of the vortex. (The case of  $\sigma = 0$  is validated against Ravichandran and Govindarajan [25].) Therefore, at some later time ( $t = 0.6\tau_\eta$ ),  $\Phi$  is essentially 0 at small values of  $r$  before sharply peaking at  $r_*$ . The onset of this peak corresponds to the flat region already noticed in Fig. 1. Understandably,  $\Phi$  falls off—less rapidly—as  $r > r_*$ . At later times, the density profile is qualitatively the same, but with a sharper peak that is shifted outward. Eventually, the profile asymptotes to a delta function, as  $t \rightarrow \infty$ , at a value of  $r_*$  where the inward flow-drag, due to stretching, is balanced by the centrifugal action of the vortex [37].

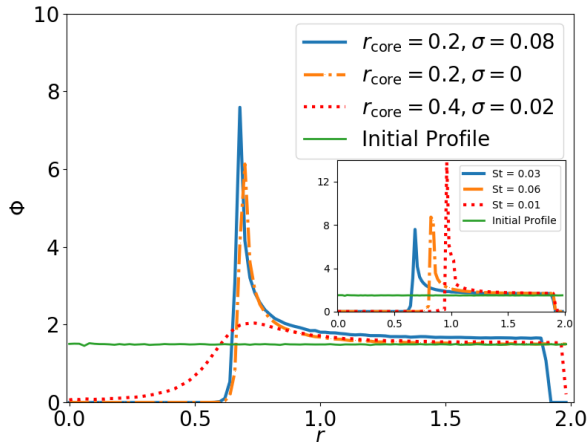


FIG. 3. (color online) Representative plot of the particle number density  $\Phi$ , for  $St = 0.03$ , as a function of  $r$  at time  $t = 0.6\tau_\eta$  for different flow geometries (see legend). The effect of particle inertia is illustrated in the inset which shows  $\Phi$  vs  $r$ , for a given flow geometry ( $r_{\text{core}} = 0.2$ ,  $\sigma = 0.08$ ), for particles with  $St = 0.03$ ,  $St = 0.06$  and  $St = 0.1$ . The horizontal, green unbroken line is the initial uniform density profile.

In Fig. 3 we also notice two distinct effects. The peak in the density profile, at any given time, is significantly sharper and more pronounced in the presence of stretching. This is because stretching counters the expulsion process due to the vortex and hence constrains particles to concentrate more sharply around  $r_*$ . Furthermore, for the weaker vortex, not only is the density profile less sharp, it also shows clearly that evacuation of particles from the vortex core is incomplete, as is also suggested by the lack of a clear plateau in Fig. 1(b).

What role does the Stokes number of the particles play in all of this? In the inset of Fig.3 we answer this question precisely, by showing the density profile for different values of  $St$ , for a given flow geometry. As we would expect, the critical distance  $r_*$  is a monotonically increasing function of the Stokes number, even in the limit  $t \rightarrow \infty$ .

This distinct and sharp profile of  $\Phi$  and the differential radial evacuation of particles from the core of the vortex must have an important bearing on the statistics of collisions—and hence coalescences—of inertial particles. In particular, it seems reasonable to assume that (a) the sharply localised high value of  $\Phi$ —and the corresponding reduction in the average inter-particle distance—ought to lead to a higher rate of collision; and (b) the differential radial velocities of particles, which depend on their initial distance from the vortex core as discussed above, would lead to larger collisional velocities than in a more quiescent, vortex-free, region of a flow. It therefore behooves us to test this conjecture in our model system. We should keep in mind that our results are meaningful only for short times: In an actual spatio-temporally varying turbulent flow, vortices are spatially localised for very short times unlike our stationary model; hence we are careful to consider only those collisions which occur at times shorter

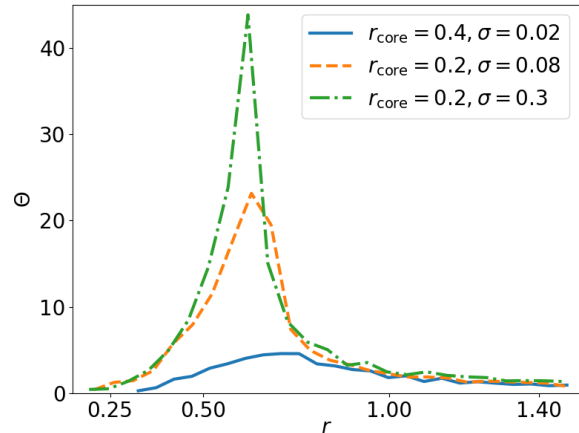


FIG. 4. (color online) Plots of the collision density  $\Theta$  (collisions occurring per unit volume) as a function of the radial distance  $r$  for different flow geometries.

than the Kolmogorov time-scale, in order for the insights we develop to have implications for realistic particle-laden flows.

We use a standard algorithm for detecting particle collisions [17, 41], and reduce the  $N_p^2$  computational cost by dividing, at every time step, the spatial domain into equal-sized grids. By optimally choosing our grid sizes, we manage to ensure that within one time step the particles do not cross more than one grid, which guarantees that no collisions are missed even when the search is limited to the particle-containing grid and its nearest neighbours. After detecting a collision, the two particles are merged, conserving mass and momentum, into a new larger particle, located at the centre of mass of the colliding pair.

We initialise 200,000 particles, with radii  $a = 2 \times 10^{-3} \approx \frac{\eta}{20}$ , randomly in a small cubic domain centered at the vortex. This results in an initial particle volume fraction of  $O(10^{-4})$  that is commensurate with the dilute situation encountered, e.g., in clouds. The particles are then evolved according to (3) up to a time  $t = 0.6\tau_\eta$ . We simultaneously detect the number of collisions  $\Theta$  which occur per unit volume, as a function of the radial distance, by considering the collisions which happen in concentric cylindrical shells parametrised by their radii  $r$ . We, as before, averaged our data over 100 independent ensembles of initial particle configurations.

Figure 4 shows a plot of  $\Theta$ , as a function of  $r$  for three representative flow geometries, namely, ( $r_{\text{core}} = 0.4$ ,  $\sigma = 0.02$ ), ( $r_{\text{core}} = 0.2$ ,  $\sigma = 0.08$ ), and ( $r_{\text{core}} = 0.2$ ,  $\sigma = 0.3$ ). (Our results from other sets of simulations with different parameters show the same qualitative behaviour.) We immediately notice more pronounced peaks in  $\Theta$  for the more intense vortices reminiscent of, and for the same reasons as, the effects we had already seen in our measurement of the particle number density  $\Phi$ . Unlike the case of number density, however, the spike in the measurement of  $\Theta$ , though clearly concentrated around  $r_*$ , is less sharp.

We also see, in Fig. 4, that an increase in the degree of

stretching  $\sigma$ —which accentuates the clustering around  $r_*$ —leads to a considerable increase in the number of collisions. However, could there be another explanation for this effect different from the one we suggest—namely the outward centrifugal forces and the inward stretching flow conspiring together? Indeed, for a three-dimensional system such as ours, it is plausible that the increase in  $\Theta$  with  $\sigma$  could be simply due to the motion of particles along the  $\hat{z}$ -axis because of the fluid velocity component  $u_z = 2\sigma z$ . To test this hypothesis, we perform simulations where we retained the radially inward flow unchanged but artificially set  $u_z = 0$ . Surprisingly, we found that a suppression of the axial flow actually results in an overall increase of approximately 12% in the peak value of  $\Theta$ , indicating that the  $\hat{z}$ -directed flow actually serves to inhibit collisions. In retrospect, this is understandable because the stretching flow pulls particles apart along the  $\hat{z}$ -direction, thereby reducing the local density and likelihood of collisions.

This is a rather interesting and important observation, which suggests that the majority of collisions, and hence coalescences, are spatially localised because of two opposite, and yet complementary effects: the centrifugal or *sling* effects of a vortex which evacuates particles *away* from the vortex, and an inward flow which actually brings-in particles *towards* the vortex. Interesting as this observation may be, it is important to be cautious about how generic this effect could be in turbulent flows. Indeed this needs to be checked and studied in more realistic flows, involving direct numerical simulations of the Navier-Stokes equations as well as gravitational effects, to be able to conjecture that the rapid growth of aggregates in very high Reynolds number flows, such as rain drops in warm clouds, owes its origin to precisely this mechanism. Our model system, nevertheless, allows us to incorporate one additional feature which is especially relevant in the understanding of droplet-growth through coalescences in clouds, namely, poly-dispersity.

We now perform simulations with an ensemble of particles whose radii  $a$  are not constant (mono-disperse) but are actually taken from a Gaussian distribution with a mean (radius)  $a_0 = 2 \times 10^{-3}$  and a standard deviation which is 10% of the mean. The Stokes numbers of these particles, naturally, are also distributed, as  $St \propto a^2$ . This ensures that different particles within the same ensemble have different dynamics, because of their differences in radii and therefore  $St$ . The result of our investigations, which extend recent work on the relative velocities of colliding particles in a bi-disperse suspension [17, 42], is instructive. In Fig. 5 we show a representative plot where we compare the collision rate  $\Theta$  of a poly-disperse suspension with that obtained for a mono-disperse suspension (where particles have the same radius as the mean radius in the poly-disperse case), in a flow with  $r_{\text{core}} = 0.4$  and  $\sigma = 0.02$ . Poly-dispersity dramatically increases the number of collisions, in spite of the vortex in this case being weak. This results from the distribution in ejection rates (each particle size has a different clustering distance  $r_*$ ), and shows a much higher value of  $\Theta$  than the mono-disperse case. An earlier study [20] had found a dramatic dependence of the caustics radius on small polydispersity. These results now show how this translates into increased rates of collision. In fact,

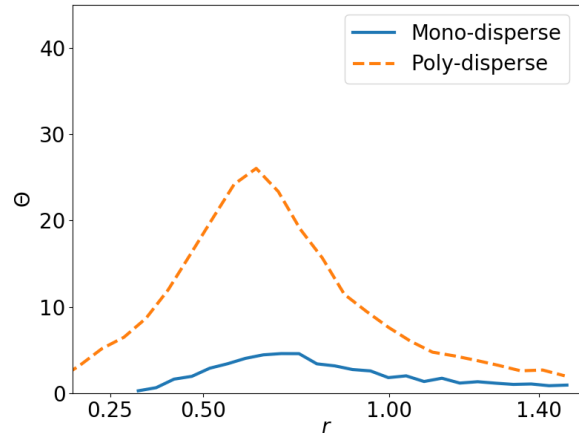


FIG. 5. (color online) Representative plots of the collision number density  $\Theta$ , as a function of  $r$ , illustrating the efficiency of a poly-disperse suspension over a mono-disperse one in facilitating collisions, and hence coalescences. We show (see text) that poly-dispersity can overcome the effect of a weak vortex and increase the value of  $\Theta$ .

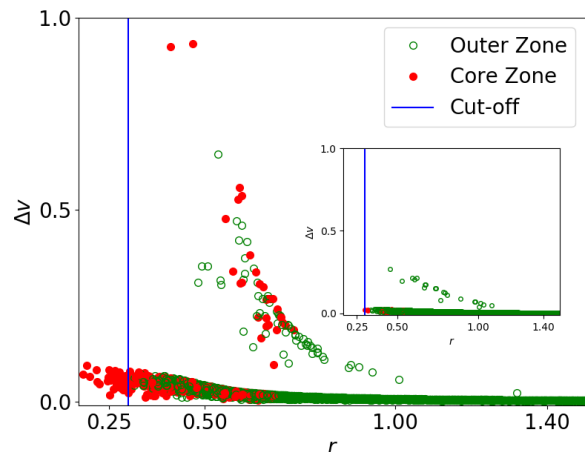


FIG. 6. (color online) A scatter plot of the relative (collisional) velocities for a small core and large core (inset) vortex corresponding to  $(r_{\text{core}} = 0.2, \sigma = 0.08)$  and  $(r_{\text{core}} = 0.4, \sigma = 0.02)$  respectively. The red, filled circles denote collisions where at least one of the colliding particles have emerged from the heart (cut-off zone) of the vortex, denoted by the blue vertical line (see text), whereas the green open circles are events where both the particles were initially outside this cut-off zone.

the  $\Theta$  with polydisperse particles is even larger than what is obtained in Fig. 4, for the mono-disperse case with a stronger vortex and a stronger inward flow ( $r_{\text{core}} = 0.2, \sigma = 0.08$ ). This result suggests that, at least in a model system, a spread in the size of droplets in a suspension—as is the case in natural systems such as clouds—triggers a more rapid growth in particle sizes through coalescences.

Our results so far, admittedly in a model flow, suggest a reasonably self-consistent picture of *where* and *how frequently* collisions occur in particle-laden flows dominated by columnar vortical structures. Before we conclude, it is useful to see what all of this means for the relative velocity  $\Delta v$  of colliding droplets as well as the contribution of the Lagrangian history of particles in determining  $\Delta v$ . This is important not only for having an estimate of how *fast* droplets hit each other, and hence whether these collisions lead to coalescences or fragmentation, but also crucial for modelling collision kernels in a mean field sense.

In Fig. 6 we show a scatter plot of  $\Delta v$  vs  $r$  corresponding to the collisions depicted in Fig. 4, for both, the small core and the large core (inset) vortices. We plot the value of  $\Delta v$  with either a red (filled) circle or a green (open) circle; the red filled circles are used when the trajectories of one or both the colliding particles start from a region very close to the vortex core, called the *cut-off* zone for convenience and shown as a vertical blue line in the figure; the green open circles are meant for those collisions that involve particles which were initially at positions outside this cut-off zone. We choose the cut-off zone to be at  $r = 0.3$ , since, as we have seen before (Fig. 1a), this corresponds to the position where the centrifugal ejection is the strongest for both the weak and strong vortices.

Our results (Fig. 6) indicate an essentially bimodal distribution of  $\Delta v$ : There are rare collisions with relatively large collisional velocities, whereas most of the collisions have much milder impacts; extremal values of  $\Delta v$  seem to be much larger for the stronger vortex than for the weaker one. Furthermore, especially for the stronger vortex, several high values of  $\Delta v$  correspond to collisions which occur due to one or both of the particles being violently ejected from the cut-off zone, and hence are marked in red filled circles. This disproportionate contribution to high-impact collisions from particles originating near the vortex core becomes clearer when we look at the numbers.

Since our particles were initially distributed randomly, only 4% of them had initial positions  $r_0$  within the vortex core. For the stronger vortex these particles contribute to approximately 17% of the collisions whereas for the weaker flow this contribution (for the same initial distribution) comes down to 2%. This is visually illustrated by comparing the number of red (filled) circles in Fig. 6 and its inset. Indeed, on average we have found that the relative velocity of collisions with particles originating from within the cut-off zone are far higher than those involving particles outside it. This strongly suggests that rapid centrifugal ejection of particles, initially close to the centres of stretched tubular vortices, lies at the heart of high velocity collisions in particle-laden, intensely turbulent flows.

#### IV. CONCLUSION

Our model, based on the premise that the singular structure of an intense vortex is a key component of high Reynolds number flows, shows the extraordinary effect of the interplay between the mechanics of centrifugal ejection and vor-

tex stretching. This shows up primarily in the spatial dependence of the particle number density  $\Phi$ . This preferential clustering—which is enhanced for strong, but stretched, vortices—has a direct bearing on collision frequencies  $\Theta$  and collisional velocities  $\Delta v$ . We also examined the role of polydispersity in our ensemble of particles and showed how, in fact, even a relatively narrow distribution of radii and Stokes times dramatically accelerates the rate of collisions, and presumably therefore, of coalescences when the colliding objects are droplets. All of this suggests the importance of the Lagrangian history of particle trajectories which lead us to uncover how extreme events—yielding high values of  $\Delta v$ —can actually be traced back to the proximity of particles to a vortex.

Before we conclude, we must confront the question of the relevance of our study—without overstating our case, keeping in mind that we study a model system—and its implications for realistic turbulent particle-laden flows. To answer this question, we recall that although our results are interesting and generic, this work was in part motivated by the *bottle-neck problem*: The question of how, starting from very small nuclei droplets that result from condensation, large aggregates of rain-forming drops grow in a warm cloud. A key ingredient in this process is coalescence, triggered by collisions, and the role of turbulent mixing. Given the very high Reynolds numbers encountered in such flows, the vorticity field is expected to be highly intermittent, with the most intense regions taking the form of stretched vortex tubes. It is therefore natural to ask what the precise role of intense vortex filaments is in the transport and collision-driven growth of particles. Hence our model.

With abundant caution, dictated by the artificial and static nature of our flow, we investigated this question with detailed numerical simulations. Our results hint strongly at the possibility that the action of stretched vortices, as well as the narrow variation in size distribution of the nuclei droplets, enhance coalescence events to a great degree. It is within this context that this work assumes special importance.

We hope that our results for this model system will trigger detailed direct numerical simulations to validate this mechanism in future studies.

#### ACKNOWLEDGMENTS

SSR acknowledges the support of the Indo–French Center for Applied Mathematics (IFCAM) and the support of the DST (India) project ECR/2015/000361. The simulations were performed on the cluster *Mowgli*. LA acknowledges the support of the INSPIRE Programme of the Department of Science and Technology, Government of India and the hospitality of ICTS-TIFR where this work was done. SR was employed at JNCASR, Bangalore, when the majority of this work was done.

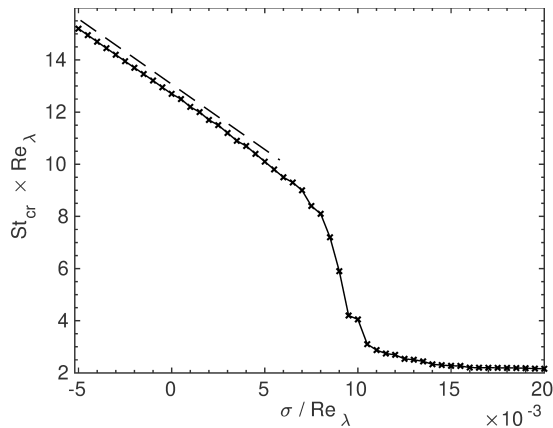


FIG. 7. The critical Stokes as a function of the nondimensional stretching rate. See, also, Fig. 2

### Appendix A: Choice of Parameters in our Numerical Simulations

A natural way in which the non-dimensional parameters for our simulations could be chosen is to set the various scales in the problem through the intrinsic time-scale  $\tau_\eta = r_{\text{core}}^2 \Gamma^{-1}$  and Reynolds number  $Re = 1/\sigma$  of the Burgers vortex model. However in this work we opt for a different strategy to make our results more testable against direct numerical simulations of highly turbulent flows or actual measurements in a physical system. We choose our model system to represent an intense vortex in a *typical* warm cloud. Hence, we consider typical, measured values of the mean-energy-dissipation rate  $\epsilon = 0.01 \text{ m}^2 \text{ s}^{-3}$ , Taylor Reynolds number  $Re_\lambda = 5000$  and kinematic viscosity  $\nu = 1.48 \times 10^{-5} \text{ m}^2 \text{ s}^{-1}$  in a turbulent warm cloud. This yields a Kolmogorov length scale  $\eta = 7.54 \times 10^{-4} \text{ m}$  and a Kolmogorov time scale  $\tau_\eta = 3.8 \times 10^{-2} \text{ s}$ . Empirically, intense, sharp, columnar vortical structures—which are mimicked by our Burgers vortex—are regions of vorticity greater than  $\sqrt{\langle \omega^2 \rangle} Re_\lambda$ , where  $\langle \omega^2 \rangle$  is the spatially averaged enstrophy given by  $\langle \omega^2 \rangle = \frac{\epsilon}{\nu}$  [28]. An estimate of the width  $l$  of such vortices suggests that  $l \approx 10\eta$ .

By using standard (dimensional) relations between the vorticity, length scale and the velocity scale,  $u = l\sqrt{\langle \omega^2 \rangle} Re_\lambda$ , we obtain the typical magnitude of the circulation of an intense vortex as  $\Gamma = l^2 \sqrt{\langle \omega^2 \rangle} Re_\lambda$ .

Adapting this phenomenology to the Burgers vortex, we set  $r_{\text{core}} = l = 7.54 \times 10^{-3} \text{ m}$  and  $\Gamma = 0.104 \text{ m}^2 \text{ s}^{-1}$  and the stretching coefficient  $\sigma = \frac{2\nu}{r_{\text{core}}^2} = 5.2 \times 10^{-1} \text{ s}^{-1}$  [39]. These parameters, which build our stretched Burgers vortex model, are of course dimensional. However, it is important for our numerical simulations to deal with dimensionless parameters. Using  $\tau_\eta$  as a time scale and  $25\eta$  as a length scale, we obtain the non-dimensional parameters for our simulations as  $\Gamma = 11.313$ ,  $r_{\text{core}} = 0.4$ , and  $\sigma = 0.02$  (corresponding to a normalized  $\tau_\eta = 1$ ). This  $r_{\text{core}}$  sets our parameters for the large core vortex. Our other parameters, listed in the main text of the paper, are variations of these obtained by keeping  $\Gamma$  fixed and applying the scaling  $\sigma \propto 1/r_{\text{core}}^2$ . In some cases however, e.g. in Figs. 1 to 3, we vary  $\sigma$  while keeping  $r_{\text{core}}$  fixed, in order to isolate the influence of the stretching flow.

The particles are characterised by their Stokes time:

$$\tau_p = \frac{2a^2 \rho_p}{9\nu \rho_f} \quad (\text{A1})$$

where  $a$  is the radius of the particle,  $\rho_p$  is the density of the particle (liquid water), and  $\rho_f$  is the density of the carrier fluid (air). Typical droplet nuclei in a warm cloud grow up to a size  $a \approx 10 \mu\text{m}$  through condensation; further rapid growth up to sizes 8 times larger, which can trigger rain, is due to coalescences. By taking typical values of the densities,  $\rho_f = 1.225 \text{ kg m}^{-3}$  and  $\rho_p = 9.97 \times 10^2 \text{ kg m}^{-3}$ , we obtain  $\tau_p = 1.22 \times 10^{-3} \text{ s}$ . This yields a Stokes number  $St = \frac{\tau_p}{\tau_\eta} = 3.17 \times 10^{-2}$ . In our simulations, we work with Stokes numbers that match this typical value, by suitably selecting values of  $\tau_p$ , keeping in mind the normalization  $\tau_\eta = 1.0$  (see above). The values of  $St_{\text{cr}}$  presented in Fig. 2 fall within this range of  $St$ , indicating that even such small particles can undergo caustics in the vicinity of strongly stretched, intense vortices. Fig. 2 was calculated for the case of  $Re_\lambda = 5000$ . For geophysical flows with higher values of  $Re_\lambda$ , we expect this effect to be further enhanced, as more intense vortices are formed. This dependence on  $Re_\lambda$  is made apparent in Fig. 7, which is a generalized version of Fig. 2.

- 
- [1] J. Bec, *Physics of Fluids* **15**, 1 (2003).
  - [2] K. V. Beard and H. T. Ochs, *J. App. Met.* **32**, 608 (1993).
  - [3] J. Bec, H. Homann, and S. S. Ray, *Phys. Rev. Lett.* **112**, 184501 (2014).
  - [4] J. Bec, S. S. Ray, E. W. Saw, and H. Homann, *Phys. Rev. E* **93**, 031102 (2016).
  - [5] M. S. Borgas and B. L. Sawford, *J. Fluid Mech.* **279**, 6999 (1994).
  - [6] S. Ravichandan, P. Deepu, and R. Govindarajan, *Sadhana* **42**, 597 (2017).
  - [7] A. Johansen, J. S. Oishi, M.-M. M. Low, H. Klahr, T. Henning, and A. Youdin, *Nature* **448**, 1022 (2007).
  - [8] K. D. Squires and J. K. Eaton, *Phys. Fluids* **3**, 1169 (1991).
  - [9] L.-P. Wang and M. R. Maxey, *J. Fluid Mech.* **256**, 2768 (1993).
  - [10] A. Wood, W. Hwang, and J. Eaton, *Int. J. of Multiphase Flow* **31**, 1220 (2005).
  - [11] S. Balachandar and J. K. Eaton, *Annu. Rev. Fluid Mech.* **42**, 111 (2010).
  - [12] R. A. Shaw, *Annu. Rev. Fluid Mech.* **35**, 183 (2003).
  - [13] J. Bec, A. Celani, M. Cencini, and S. Musacchio, *Phys. Fluids* **17**, 1 (2005).
  - [14] G. Falkovich and A. Pumir, *J. Atmos. Sciences* **64**, 4497 (2007).
  - [15] J. Bec, S. Musacchio, and S. S. Ray, *Phys. Rev. E* **87**, 063013 (2013).

- [16] A. Pumir and M. Wilkinson, *Annu. Rev. Cond. Matt. Phys.* **7**, 141 (2016), 1508.01538.
- [17] M. James and S. S. Ray, *Sci. Rep.* **7**, 12231 (2017).
- [18] E.-W. Saw, G. P. Bewley, E. Bodenschatz, S. S. Ray, and J. Bec, *Phys. Fluids* **26**, 111702 (2014).
- [19] J. R. Picardo, L. Agasthya, R. Govindarajan, and S. S. Ray, *Phys. Rev. Fluids* **4**, 032601 (R) (2019).
- [20] P. Deepu, S. Ravichandran, and R. Govindarajan, *Phys. Rev. Fluids* **2**, 024305 (2017).
- [21] M. R. Maxey, *J. Fluid Mech.* **174**, 441465 (1987).
- [22] G. Falkovich, A. Fouxon, and M. G. Stepanov, *Nature* **419**, 151 (2002).
- [23] M. Wilkinson, B. Mehlig, and V. Bezuglyy, *Phys. Rev. Lett.* **97**, 048501 (2006).
- [24] G. P. Bewley, E.-W. Saw, and E. Bodenschatz, *New J. Phys.* **15**, 083051 (2013).
- [25] S. Ravichandran and R. Govindarajan, *Phys. Fluids* **27** (2015).
- [26] J. M. Burgers, *Advances in Applied Mechanics* (Academic, New York, 1948, 1948).
- [27] Z. She, E. Jackson, and S. A. Orszag, *Nature* **344**, 226 (1990).
- [28] J. Jiménez and A. A. Wray, *J. Fluid Mech.* **373**, 255 (1998).
- [29] T. Ishihara, Y. Kaneda, M. Yokokawa, K. Itakura, and A. Uno, *J. Fluid Mech.* **592**, 335366 (2007).
- [30] S. Douady, Y. Couder, and M. E. Brachet, *Phys. Rev. Lett.* **67**, 983 (1991).
- [31] T. S. Lundgren, *Phys. Fluids* **25**, 2193 (1982).
- [32] J. Gibbon, A. Fokas, and C. Doering, *Physica D* **132**, 497 (1999).
- [33] B. Galanti, J. Gibbon, and M. Heritage, *Nonlinearity* **10**, 1675 (1997).
- [34] J. Gibbon and M. Heritage, *Phys. Fluids* **9**, 901 (1997).
- [35] S. J. Chapman, C. M. Elliott, A. K. Head, S. D. Howison, F. M. Leslie, J. R. Ockendon, and P. G. Saffman, *Philosophical Transactions of the Royal Society of London. Series A: Mathematical, Physical and Engineering Sciences* **355**, 1949 (1997).
- [36] M. Wilczek, F. Jenko, and R. Friedrich, *Phys. Rev. E* **77**, 056301 (2008).
- [37] B. Marcu, E. Meiburg, and P. K. Newton, *Physics of Fluids* **7**, 400 (1995).
- [38] R. J. Hill, *Phys. Fluids* **17**, 037103 (2005).
- [39] P. A. Davidson, *Turbulence: An Introduction for Scientists and Engineers* (Oxford University Press, UK, 2004).
- [40] M. R. Maxey, *Phys. Fluids* **26**, 883 (1983).
- [41] S. Sundaram and L. R. Collins, *J. Fluid Mech.* **335**, 75109 (1997).
- [42] A. Bhatnagar, K. Gustavsson, B. Mehlig, and D. Mitra, *Phys. Rev. E* **98**, 063107 (2018).